PCCP

Accepted Manuscript

ROYAL SOCIETY OF CHEMISTRY

www.rsc.org/pccp

A Hybrid DFT Based Investigation of Photocatalytic Activity of Cation-Anion codoped $SrTiO_3$ for Water Splitting under Visible Light

Brindaban Modak, K. Srinivasu and Swapan K. Ghosh*

Theoretical Chemistry Section, Bhabha Atomic Research Centre
and Homi Bhabha National Institute, Mumbai – 400 085, India

Email: skghosh@barc.gov.in

Phone: 91-22-25595092

Fax: 91-22-25505151

Abstract

In this study, effect of cation (Mo or W) and anion (N) codoping on the band structure of $SrTiO_3$ is investigated to improve its photocatalytic activity for water splitting under sun light. We consider both the non-compensated and compensated codoping strategies using different ratio of the cationic and anionic dopant. Present study employs hybrid density functional theory to describe the electronic structure of all the systems accurately. Although, non-compensated (1:1) codoping reduces the band gap significantly, presence of localized impurity states may hinder charge carrier mobility. This also changes the positions of the band edges in such an extent that the (Mo/W, N)-codoped $SrTiO_3$ system becomes ineffective for overall water splitting. Besides, formation of charge compensating defects may contribute to the carrier loss. On the other hand, compensated (1:2) codoping not only reduces the band gap to shift the absorption curve towards visible region, but also passivates the impurity states completely, ensuring improved photoconversion efficiency. The reduction of band gap is found to be more prominent in case of (W, 2N)-codoped $SrTiO_3$ than (Mo, 2N)- codoped $SrTiO_3$. In both the cases, the band edge positions are found to satisfy the thermodynamic criteria for overall water splitting. Our calculation predicts that the codoping of (Mo/W) and N in 1:2 ratio also enhances the reducing property at the conduction band in comparison to that in the undoped $SrTiO_3$, which is beneficial for hydrogen release in the water splitting. Present study thus demonstrates the effect of nature of the dopant elements as well as their proportion to achieve the best outcome of the designed material for practical applications.

Keywords: $SrTiO_3$, Hybrid Density Functional, Water splitting, Cation-anion codoping

1. Introduction

Development of photocatalyst that can generate hydrogen via water splitting under sunlight, or destroy environmental pollutants is one of the major areas of interest during past decades.[1-7] An ideal photocatalyst should have long term stability, lower band gap to utilize the solar spectrum, and proper band edge positions to meet the thermodynamic criterion for water splitting. Besides these aspects, the mobility of the photo-generated charge carriers should also be good enough for high photoconversion efficiency. However, in reality it is very difficult to obtain such a photocatalyst which satisfies all the criteria. As for example, the metal-oxide materials like TiO_2, $SrTiO_3$, $NaTaO_3$, etc. are reported to be efficient photocatalyst for water splitting.[6-11] Due to large band gap, they are however not able to show photoactivity under visible light, which constitutes the major fraction of the solar spectrum. On the other hand, WO_3 can absorb visible light, but is ineffective for hydrogen evolution due to improper conduction band edge position with respect to water reduction level.[12] These led to growing interest in band structure engineering in recent years. In the present study, our aim is to improve the visible light activity of $SrTiO_3$, which has been extensively studied for water splitting as well as degradation of environmental pollutants.[13-15] The advantages of $SrTiO_3$ are that it is highly robust and can split water even in absence of external bias potential.[16] The band gap of $SrTiO_3$ has been reported to be 3.20 eV with the conduction band maximum (CBM) lying 0.80 eV above the water reduction (H^+/H_2) level and the valence band minimum (VBM) locating 1.17 eV below the water oxidation (H_2O/O_2) level.[17, 18] There exist lots of reports exploring different strategies to shift the absorption region of $SrTiO_3$, mainly by introducing foreign element/elements in any of the two cationic sites (Sr and Ti) or in the anionic lattice site (O). Among nonmetal doping, effect of N

has been studied by several experimental as well as theoretical groups.[19-25] A series of N-doped $SrTiO_3$ with varying N concentration have been synthesized by Wang et al and significant improvement of photocatalytic activity has been observed during the oxidative elimination of nitric oxide.[23] It has been pointed out that this enhancement of visible light activity is attributed to the presence of N-induced localized mid gap states which reduce the effective band gap.[24, 25] However, these states are considered to be detrimental for the photocatalytic activity as they can hinder the charge carrier mobility and thus reduce the photoconversion efficiency.[26] Besides, defects like oxygen vacancy are known to be formed spontaneously to compensate for the charge imbalance in N-doped oxide semiconductor, may trap photo-generated electron-hole pair and accelerate their recombination.[27, 28] In case of cation doping, substitution of the transition metal element has been shown to enhance the visible light activity. As for example, Cr-doped $SrTiO_3$ has been studied by several groups for significant lowering of band gap.[29-33] It has been reported that Cr-doping reduces the band gap by introducing localized 3d states, which in turn makes it inactive for overall water splitting.[33] Other metal cations of interest for this purpose include Mn, Ru, Rh, Pb, Ag, Ir, Pd and Pt.[34-37] Although they are able to shift the absorption spectra towards the visible region, there are cases, where hydrogen evolution has not been observed at all.[35] This may be due to, as emphasized in previous studies, large perturbation at the band edge positions associated with introduction of undesirable localized states in the forbidden region.[36] Nowadays, codoping approach has been shown to be one of the successful approaches in designing new photocatalyst with improved photoresponse.[38-41] This has also been shown to be popular for improving the photocatalytic activity of $SrTiO_3$ involving either anion-cation, anion-anion, or cation-cation pairs.[42-48] Recently, significant attention has been paid to improve the photocatalytic activity of N-doped $SrTiO_3$ by introducing either a nonmetal (H, F, Cl, Br, I) or a

metal (Cr, V, Nb, Ta, Sc, Y, La) as a codopant.[42-45] Although they are found to be successful in suppressing the N-induced undesirable states by forming charge compensated system, their potentiality towards overall water splitting is still to be tested.

In this study, we have adopted metal-nonmetal codoping approach to improve the photocatalytic behavior of $SrTiO_3$ under visible light. While choosing the codopant pair for this purpose, we consider some important aspects, viz., (a) they should not bring significant distortion in parent crystal structure, (b) they should reduce the band gap to such an extent that the visible light absorption will be appreciable, (c) they should not perturb the CB edge of $SrTiO_3$ significantly to make large downward shifting, (d) they should not introduce discrete mid gap states. We carefully choose Mo and W for the Ti lattice site and N for the O lattice site due to similarity in their ionic sizes. As the energy of N 2p orbital is higher than the O 2p orbital, N doping is effective for elevation of the valence band maximum (VBM). In fact, it has been successfully shown that the codoping of Mo/ W and N significantly increases the photocatalytic activity of TiO_2 under visible light.[49-52] The substitution of N ($2s^2 2p^3$) for O ($2s^2 2p^4$) will add one hole to the system, while substitution of Mo ($5s^2 4d^4$) or W ($6s^2 5d^4$) for Ti ($4s^2 3d^2$) will add two extra electrons. Hence, equimolar proportion 1:1 of both the dopant elements, Mo/W and N will lead to the formation of a non-compensated codoped system. However, to form a compensated codoped system the proportion of Mo/W and N should be 1:2. Since the photocatalytic property may alter with the type of codoping, viz., compensated or non-compensated, we have studied here both the varieties. We employ density functional theory (DFT) as a tool for the quantum chemical calculations. The stability of the proposed codoped system has been assessed by calculating the defect pair binding energies. An accurate description of the electronic structure has been presented by using sophisticated hybrid functional as prescribed by Heyd, Scuseria, and

Ernzerhof (HSE).[53] The change in electronic structure has been explored by plotting density of states (DOS) and projected density of states (PDOS). Applicability of these materials for the photo-splitting of water is assessed by aligning the band edges with respect to the water redox levels. To have a look at the spectral shift we plot the optical absorption curve. We also find favorable growth condition for the modified systems.

2. Computational Details

All the DFT calculations have been performed using VASP electronic structure code.[54] The valence electron and ion core interactions have been described by projector augmented wave (PAW) potential.[55] The exchange and correlation energy density functional is considered under the framework of generalized gradient approximation (GGA) with Perdew-Burke-Ernzerhof (PBE) scheme.[56] Brillouin zone has been sampled with sufficient number of Γ-centered k-point sets generated based on Monkhorst and Pack scheme.[57] The cutoff energy of 600 eV defines the limit to expand the electronic wave function in plane wave. The doped systems have been modeled using supercell of the cubic $SrTiO_3$ crystal structure (space group: $P\,m\,\bar{3}\,m$). All the geometries have been fully relaxed with a k-point mesh of 8 × 8 × 8. During geometry optimization the residual forces on the atoms are allowed to converge to a value smaller than 0.01 eV/Å and the self consistent iteration continues until the tolerance for total energy reaches 10^{-6} eV. All the electronic property calculations have been carried out with HSE hybrid density functional, for which the exchange and correlation energy maintains the relation below

$$E_{XC}^{HSE} = a\,E_X^{SR}(\mu) + (1-a)\,E_X^{PBE,\,SR}(\mu) + E_X^{PBE,\,LR}(\mu) + E_C^{PBE}, \qquad (1)$$

where 'a' and 'μ' define the mixing coefficient and the screening parameter, respectively. We consider 28 % of mixing for the exchange and 0.2 $Å^{-1}$ for the screening parameter, reported to calculate the band gap of $SrTiO_3$ very close to the experimental value.[33, 48] A k-point mesh of 3 × 3 × 3 has been used for the electronic property calculation with the HSE functional. The valence states included for the construction of PAW potential are: Sr ($4s^2 4p^6 5s^2$), Ti ($4s^2 3d^2$), Mo ($5s^2 4d^4$), W ($6s^2 5d^4$), O ($2s^2 2p^4$), and N ($2s^2 2p^3$). Frequency dependent dielectric function calculation has been employed as implemented in VASP to get the optical spectrum. The condition of spin polarization has been implemented throughout the calculations reported here.

3. Results and Discussions

3.1. Geometry and Electronic Structure

At room temperature pure $SrTiO_3$ belongs to cubic perovskite structure (Fig. 1), where Ti atom is octahedrally surrounded by six oxygen atoms. To obtain a detailed insight into the effect of the dopants on the electronic structure of $SrTiO_3$, we have calculated the DOS and PDOS for all the model systems. For the undoped $SrTiO_3$, the VBM and CBM are composed of mainly O 2p states and Ti 3d states (Fig. 2), respectively. The calculated band gap is found to be 3.19 eV, which is very close to the experimentally reported value (3.20 eV).[17] This observation encourages our choice of calculation method for computational design of modified $SrTiO_3$ catalyst. To model N-doped $SrTiO_3$ one of the O atoms from the 2 × 2 × 2 supercell is replaced by N atom, which corresponds to a dopant concentration of 4.17%. We consider two different configurations, where the N atom occupies either O1 or O2 lattice site (Fig. 1). The introduction of N at the O1 lattice site is found to be energetically more favorable by 0.005 eV in comparison to that at the O2 lattice site. In the optimized geometry of N-doped $SrTiO_3$, the Ti-N bond length

(1.976 Å) is found to be very close to the Ti-O bond length (1.974 Å) in undoped $SrTiO_3$. As the valence cell of N contains one less electron than that in O, it will introduce one hole to the system. The DOS plot (Fig. 3a) shows that N doping introduces partially occupied states 0.73 eV above the valence band (VB) and unoccupied states 1.13 eV below the conduction band (CB). This is the consequence of higher energy of the N 2p orbital than O 2p orbital. Therefore the band gap reduces to 2.31 eV, which provides an explanation of the experimental observation of improved visible light activity of N-doped $SrTiO_3$.[23] However, the localized unoccupied states may serve as electron-hole recombination centre. To investigate the effect of increasing concentration, we introduce two N atoms at the O1 and O2 lattices sites (Fig. 1). The (N, N)-doped $SrTiO_3$ is deficient by two electrons. The change in crystal structure is found to be small even in presence of higher N concentration (8.33 %). The calculated (N, N) distance is found to be 2.663 Å, which is shorter than the (O, O) distance (2.792 Å) in the undoped $SrTiO_3$. The electronic structure (Fig. 3b) in this case is characterized by the presence of the fully occupied impurity states near the VB and unoccupied states near to the CB. Higher concentration of N results formation of continuum states at the band edges. As the unoccupied states are very close to the CB, we assume the band gap as the difference between these unoccupied states and the VB, and calculated as 1.58 eV. Although, increasing concentration improves the visible light activity, significant downward shifting of the CB edge may affect the reducing behavior severely. Now we will discuss the effect of doping with only Mo/ W on the electronic structure of $SrTiO_3$. The Mo/W-doped $SrTiO_3$ modeled by introducing Mo or W at the Ti1 lattice site (Fig. 1) of the 2 × 2 × 2 supercell, corresponds to a dopant concentration of 12.5 %. Due to similarity in ionic size between the host element (R_{Ti+4}= 0.605 Å) and the substituent element (R_{Mo+6}= 0.59 Å and R_{W+6}= 0.60 Å) the perturbation in the cubic structure is found to be very small.[58] The

calculated Mo-O bond length (d_{Mo-O}= 1.972 Å) is comparable to the Ti-O bond length (d_{Ti-O}= 1.974 Å). However, Mo introduces partially occupied impurity states just below the CB (Fig. 4a). This is due to presence of two more electrons in the valence cell of Mo ($5s^2\ 4d^4$) than that in Ti ($4s^2\ 3d^2$). Since these donor states are closer to the CBM, we assume the band gap as the difference between the VBM and the occupied impurity states, which is calculated as 1.86 eV. In case of doping with W, the calculated W-O bond distance (d_{W-O}= 1.948 Å) is found to slightly shorter than the Ti-O bond length in undoped $SrTiO_3$. The characteristic of DOS (Fig. 4b) is found to be almost similar to the case of Mo-doped $SrTiO_3$. However, the impurity states are appeared as continuous state at the conduction band edge, rather than collection of isolated states as appeared in the case of Mo-doped $SrTiO_3$. Analysis of PDOS indicates that, the impurity states are composed of hybridized states of Ti 3d state and W 5d state, i.e., the mixing of Ti 3d states and W 5d states is relatively stronger in this case. This can be interpreted by the closeness of the Ti 3d orbital energy to the W 5d orbital energy, while differs significantly from Mo 4d orbital energy. The effective band gap for W-doped $SrTiO_3$ is calculated as 2.40 eV. Although, from the point of band gap narrowing, doping with only Mo/W seems to be attractive, the presence of partially occupied impurity states as well as formation of charge compensating defects are the limiting factors for the improvement of photocatalytic performance. Now, we examine the scenario when both the anionic dopant and cationic dopant are present in the same supercell.

We start this discussion with 1:1 (Mo/W, N)-codoped $SrTiO_3$, which is constructed by replacing one Ti and one O atom from the 2 × 2 × 2 supercell with one Mo/W and N, respectively (dopant concentration N is 4.17 % for N-doping and is 12.5% for Mo/W doping). Here we have considered two different configurations. In one case the dopant elements are

directly attached to each other (occupying Ti1 and O1 lattice sites), while in the other configuration, they are far away from each other (occupying Ti1 and O3 lattice sites). The (Ti1, O1) configuration is found to be energetically more stable [0.96 eV and 0.78 eV for the (Mo, N)-codoped $SrTiO_3$ and (W, N)-codoped $SrTiO_3$, respectively] than the (Ti1, O3) configuration. In the present study, we are interested only in the lowest energy configuration. As Mo/W leaves two more electrons and N introduces only one hole, the (Mo/W, N)-codoped $SrTiO_3$ is charge non-compensated and is excess by one electron. The Mo-N bond distance (d_{Mo-N}= 1.762 Å) in the (Mo, N)-codoped $SrTiO_3$ is found to be significantly shorter than the Ti-N bond length (d_{Ti-N}=1.976 Å) in the N-doped $SrTiO_3$. Fig. 5a shows the DOS plot for (Mo, N)-$SrTiO_3$. Although, presence of Mo is found to be effective in passivating the N-induced acceptor states completely, partially occupied Mo-4d states are introduced in between VB and CB. Due to lower Mo 4d orbital energy with respect to Ti 3d orbital energy, it appears as discrete state, far below the CB. The CBM is hardly affected by this codoping, and still have Ti 3d character. Although these partially occupied impurity states reduce the excitation energy to 1.06 eV, they may reduce the photoconversion efficiency by trapping the charge carriers. Now we will discuss the case of W and N doping in 1:1 proportion. In the optimized geometry of (W, N)-codoped $SrTiO_3$ the W-N distance is calculated as 1.809 Å. The DOS plot for the (W, N)-codoped $SrTiO_3$ has been shown in the Fig. 5b. In contrast to the previous case, partially occupied impurity states are appeared just below the CB. This is again due to closeness in energy of the Ti 3d orbital and W 5d orbital. However, the nature of VBM is almost similar to the case of (Mo, N)-codoping. The energy difference between the VBM and the occupied impurity state is calculated as 2.07 eV. Although, in this case no discrete state in between VB and CB are observed, the impurity states significantly lower the CBM and thus may affect the reducing behavior severely. Besides, non-

compensated codoping is accompanied by the formation of vacancy states, which are known to be efficient source for electron-hole recombination. Hence, 1:1 (Mo/ W, N)-codoped $SrTiO_3$ may show poor photocatalytic performance.

To overcome these problems, we have considered charge compensated (Mo/W, 2N)-codoped $SrTiO_3$. The (Mo/W, 2N)- $SrTiO_3$ is modeled with 2 × 2 × 2 supercell by introducing one Mo/W and two N in the Ti and O lattice sites, respectively (dopant concentration for Mo/W is 12.5 % and for N it is 8.33 %). In this case, we consider three different configurations obtained by varying the substitution sites for the dopant elements, viz.: (Ti1, O1, O2), (Ti1, O1, O3) and (Ti3, O1, O2). The (Ti1, O1, O2) configuration, where both the N occupy nearest neighboring lattice sites of Mo (W) is found to be energetically more stable by 0.75 eV (0.56 eV) than the (Ti1, O1, O3) configuration and 2.06 eV (1.50 eV) than the (Ti3, O1, O2) configuration. Here, we describe the electronic structure of the lowest energy configuration for both the cases. The calculated Mo-N bond distances (d_{Mo-N} = 1.800 Å and 1.808 Å) and W-N bond distances (d_{W-N} = 1.825 Å and 1.840 Å) in these cases are found to be slightly longer than that in their 1:1 analogues. The N, N distance (d_{N-N} = 2.803 Å and 2.814 Å) in both cases is found to be longer than that in 2N- $SrTiO_3$ (d_{N-N} = 2.663 Å), while closer to the corresponding O, O distance (d_{O-O} = 2.792 Å) in the undoped $SrTiO_3$. This may be due to isolelectronic nature of the (Mo/W, 2N)-codoped $SrTiO_3$ with the undoped $SrTiO_3$. The DOS plot (Fig. 6) shows that the Fermi level is shifted to the top of the VB, i.e., both (Mo, 2N)-$SrTiO_3$ and (W, 2N)-$SrTiO_3$ systems will behave as intrinsic semiconductor. It is interesting to observe that both the impurity induced states are completely passivated in these cases, ensuring improved charge carrier mobility as well as photoconversion effieciency due to elimination of the local trapping centers. As the (Mo/W, 2N) codoped $SrTiO_3$ being a charge compensated system, vacancy related defects formation is

expected to minimum, which is beneficial for lower electron-hole recombination rate. Analysis of PDOS indicates that the nature of CBM is similar in both the cases. However, the characteristics of the VBM for (Mo, 2N)-codoped $SrTiO_3$ and (W, 2N)-codoped $SrTiO_3$ differs significantly. In case of (Mo, 2N)-codoped $SrTiO_3$ the VBM is composed of (N 2p, O 2p) hybridized state, with the majority contribution from O 2p state. While, in case of (W, 2N)-codoped $SrTiO_3$ the VBM is dominated by N 2p state. Analysis of energy levels indicates that the lowering of N 2p orbital energy occurs in larger extent in presence of Mo than that in presence of W. Consequently the band gap for (Mo, 2N)-codoped $SrTiO_3$ (2.82 eV) differs from that of (W, 2N) codoped $SrTiO_3$ (2.62 eV). To investigate this in more details we analyze the charge density distribution (Fig. 7). In case of (Mo, 2N)-codoped $SrTiO_3$ (Fig. 7a), N electron density is found to be more delocalized towards Mo and a significant overlapping of electron cloud is observed. While, in case of (W, 2N) codoped $SrTiO_3$, although the N electron density is polarized towards W, there is no significant overlapping of the electron cloud. This indicates the higher degree of covalent character in the bonding between Mo and N than that in between W and N. This is again supported by Bader charge density analysis. [59] The calculated Bader charges on the N centers are -1.27 |e| and -1.26 |e| for (Mo, 2N)-codoped $SrTiO_3$, while -1.38 |e| and -1.37 |e| for (W, 2N)-codoped $SrTiO_3$. We should also point out that the band gap narrowing in both the cases are the result of elevation of VBM only, as the CBM also moves to the upward direction. This also justifies the choice of our doping strategy to improve the photocatalytic behavior of $SrTiO_3$, for which the CBM is only 0.80 eV above the water reduction level.

3.2. Defect Pair Binding Energy

To obtain an insight into the coupling strength between the impurity species in the codoped $SrTiO_3$ we have calculated the defect pair binding energy (E_b), defined as

$$E_b = E_{\text{mono-doped (X@O)}} + E_{\text{mono-doped (Y@Ti)}} - E_{\text{codoped}} - E_{SrTiO3} \quad (2)$$

where E represents the total energy of the respective systems calculated for the same supercell size. The calculated binding energies for the (Mo, N)-$SrTiO_3$ and (W, N)-$SrTiO_3$ systems are 2.27 eV, and 2.31 eV, respectively. The binding energies are relatively higher in case of (Mo, 2N)- $SrTiO_3$ (4.04 eV) and (W, 2N)- $SrTiO_3$ (4.03 eV) systems. The positive binding energies indicate that the codoped systems are sufficiently stable. The extra stabilization in case of 1:2 codoping may be due to formation of charge compensated system.

3.3. Photocatalytic Activity

Up to now, we have discussed how this codoping approach is successful in reducing the band gap (enhancing visible light activity) of $SrTiO_3$. But to be suitable for water splitting process, the band edges of the codoped $SrTiO_3$ must be located in proper positions. The CB edge must be above the water reduction level (H^+/H_2) and the VB edge must be below the water oxidation level (H_2O/O_2) to satisfy the thermodynamic criterion for the hydrogen release and oxygen release, respectively. For $SrTiO_3$ the CB edge has been experimentally reported to be 0.80 eV above and the VB edge is 1.17 eV below the respective levels, fully meeting the thermodynamic criterion for overall water splitting.[18] To check the criterion for both non-compensated and compensated codoped $SrTiO_3$ we align their band edges. We first fix the positions of the CBM and VBM for the undoped $SrTiO_3$ with respect to the water redox levels based on the experimental data. Then the CBM and VBM for the modified $SrTiO_3$ systems are placed according to the relative shift of the corresponding energy levels with respect to that of the undoped $SrTiO_3$. As shown in Fig. 8, the VB edge of (Mo, N)- $SrTiO_3$ is located above the water

oxidation level (H_2O/O_2). Hence, (Mo, N)-codoped $SrTiO_3$ will not able to release O_2 in the water splitting process. While, in case of the (W, N)-codoped $SrTiO_3$ the CB edge lies very close to the water reduction level. This indicates that the (W, N)-codoped $SrTiO_3$ may not be suitable for hydrogen production through water splitting. On the other hand, the band edge positions for both (Mo, 2N)- $SrTiO_3$ and (W, 2N)- $SrTiO_3$ are such that they are suitable for overall water splitting. Figure 8 indicates that the CBM for both the systems are located even above that of the undoped $SrTiO_3$, resulting into an enhancement of reducing power as well. Thus, the (Mo, 2N)-codoped $SrTiO_3$ and (W, 2N)-codoped $SrTiO_3$ systems are expected to be thermodynamically more suitable for H_2 evolution in comparison to the undoped $SrTiO_3$.[60]

3.4. Optical Property

In this section, we discuss the extent of optical shift towards visible region due to codoping with (Mo or W) and N in 1:2 proportions. We calculate the frequency dependent complex dielectric function, $\varepsilon_1(\omega) = \varepsilon_1(\omega) + i\varepsilon_2(\omega)$. In our calculation the real part (ε_1) of the dielectric tensor is evaluated from Kramers–Kronig transformation, and the imaginary part (ε_2) from summation over the empty states. For the absorption coefficient we use the following relation [60]

$$\alpha(\omega) = \sqrt{2}\omega\left(\sqrt{\varepsilon_1(\omega)^2 + \varepsilon_2(\omega)^2} - \varepsilon_1(\omega)\right)^{1/2} \qquad (3)$$

Figure 9 shows the calculated absorption curves for the undoped $SrTiO_3$, (Mo, 2N)-$SrTiO_3$, and the (W, 2N)-$SrTiO_3$. The absorption curves for both the codoped systems are extended to the visible region with respect to that of the undoped $SrTiO_3$. This is due to decrease in photo-excitation energy with codoping as discussed in the electronic structure part. The absorption shift for the (W, 2N)-$SrTiO_3$ is relatively higher than that of the (Mo, 2N)-$SrTiO_3$.

Hence, (W, 2N) codoping should be better choice to achieve more enhancement in the visible light activity.

3.5. Defect Formation Energy

We have also calculated the formation energy for the monodoped as well as the codoped $SrTiO_3$ to explore the optimal growth condition in each case. The defect formation energy depends on the chemical potential of the host and the defect element as[62,63]

$$\Delta H_f = E_{doped} + n_O \mu_O + n_{Ti} \mu_{Ti} - E_{SrTiO3} - n_N \mu_N - n_{Mo/W} \mu_{Mo/W} \quad (4)$$

where E_{doped} is the total energy of the $SrTiO_3$ supercell containing the dopant element/elements. μ_X represents the chemical potential of the element X, and n_X indicates the number of atoms of the element X added or replaced.

At the condition of equilibrium between the $SrTiO_3$ and the reservoirs of Sr, Ti and O, their chemical potentials must follow the relation

$$\mu_{Sr} + \mu_{Ti} + 3\mu_O = \mu_{SrTiO3(bulk)} \quad (5)$$

Again the chemical potentials of the elements Sr, Ti and O cannot exceed the corresponding chemical potential in the bulk. Thus, one has $\mu_{Sr} \leq \mu_{Sr(bulk)}$, $\mu_{Ti} \leq \mu_{Ti(bulk)}$ and $\mu_O \leq \mu_{O(gas)}$. The heat of formation of bulk $SrTiO_3$ is given by

$$\Delta = \mu_{SrTiO3(bulk)} - \mu_{Sr(bulk)} - \mu_{Ti(bulk)} - 3\mu_{O(gas)} \quad (6)$$

As the Δ value for $SrTiO_3$ is negative, μ_{Sr}, μ_{Ti}, and μ_O follow the relations

$$\mu_{Sr(bulk)} + \Delta \leq \mu_{Sr} \leq \mu_{Sr(bulk)} \quad (7a)$$

$$\mu_{Ti(bulk)} + \Delta \leq \mu_{Ti} \leq \mu_{Ti(bulk)} \quad (7b)$$

$$3\mu_{O(gas)} + \Delta \leq 3\mu_O \leq 3\mu_{O(gas)} \quad (7c)$$

In the present study, $\mu_{Sr(bulk)}$ and $\mu_{Ti(bulk)}$ have been calculated from the energy of the respective atoms in their pure bulk metallic states. $\mu_{O(gas)}$ is calculated from the energy of an oxygen atom in the gaseous O_2 molecule placed at the centre of a 20 x 20 x 20 $Å^3$ cubic box. Similarly μ_N has been calculated as $\mu_N = ½\ \mu_{N2(gas)}$. For μ_{Mo} and μ_W, we have taken the energy of a Mo/W atom in the bulk molybdenum/tungsten metal.

The formation energy for the monodoped and codoped $SrTiO_3$ has been shown in Fig. 10 as a function of the chemical potential of the host element. The dopant formation energy follows an increasing trend with the chemical potential of the host element (Figs. 10a and 10b). This is due to the fact that the host rich condition is unfavorable for vacancy formation, required for the insertion of the dopant element. As can be seen from Fig. 10b, that the introduction of W in the $SrTiO_3$ crystal structure is more feasible than that of Mo. Figures 10c and 10d indicate that introduction of N in the $SrTiO_3$ crystal lattice is facilitated by the presence of Mo/W, i.e. codoping is energetically more favorable. This may be due to the stronger coupling between Mo/W and N. The formation energy for the codoped system is found to be much lower when the growth condition is O-rich rather than Ti-rich.

3.6. Effect of Concentration

To investigate the effect of concentration calculation with different super cell size has been carried out. We consider two higher concentration cases using 2 × 1 × 1 supercell and 2 × 2 × 1 supercell and one lower concentration case using 2 × 2 × 3 supercell. Here we will discuss the case of codoping with W and N in 1:2 proportion. In each case, we consider the geometry, where both the N are directly attached to W, has been found to be lowest energy configuration for the 2 × 2 × 2 supercell. In case of 2 × 1 × 1 supercell, the dopant concentration corresponds to 50 %

for W and 33.33 % for N. The calculated band gap is drastically reduced to 0.78 eV. The DOS plot has been presented in Fig. 11a. The VBM is elevated by 1.58 eV and the CBM is lowered by 0.83 eV with respect to that of the undoped $SrTiO_3$ due to higher concentration of the dopant. Hence, this highly doped $SrTiO_3$ may not be suitable for both water oxidation and reduction. In case of 2 × 2 × 1 supercell the dopant concentration corresponds to 25 % for W and 16.67 % for N. The calculated band gap (2.65 eV) is found to be close to that obtained using 2 × 2 × 2 supercell. Comparison of Fig. 11b with Fig. 6b indicates that the nature of the band edges is almost similar in both the cases. For lower dopant concentration we increase the supercell size to 2 × 2 × 3, which corresponds to the dopant concentration of 8.33 % for W and 5.55 % for N. The DOS plot has been shown in Fig. 11c and the calculated band is 2.66 eV. This indicates that even at lower dopant concentration the reduction of band gap is quite significant to achieve appreciable visible light activity. Moreover, in all the cases the impurity induced states are completely passivated to form continuous band structure at the band edges.

4. Conclusion

In this theoretical study, we investigate using hybrid DFT, the effect of codoping of Mo/W and N in different proportions aiming at improving the photocatalytic activity of $SrTiO_3$ under visible light. Presence of Mo or W favors the N-doping by reducing the formation energy. In the codoped systems, strong coupling between N and Mo or W is established, making the systems sufficiently stable. In case 1:1 codoping, although the band gap decreases significantly, incomplete passivation of the localized impurity states may lead to poor photocatalytic response. The band edge positions are also perturbed significantly, making (Mo, N)- $SrTiO_3$ inactive for oxygen evolution and (W, N)- $SrTiO_3$ unsuitable for hydrogen evolution in the water splitting process. As the (Mo/W, N)- $SrTiO_3$ is charge non-compensated, carrier loss due to defect states

may not be avoided. Thus codoping of Mo/W and N in 1:1 proportion should not be suggested for the improvement of photocatalytic efficiency of $SrTiO_3$ towards solar water splitting. On the other hand, introduction of Mo/W and N in 1:2 proportion results charge compensated codoped system, which is isoelectronic with the undoped $SrTiO_3$ and both the dopant-induced localized states are completely passivated. Hence good mobility behavior as well as improved photoconversion efficiency are expected in the (Mo/W, 2N) $SrTiO_3$ system. The reduction in band gap is solely due to the elevation of the VBM. The CBM is also found to be shifted in the upward direction, indicating that the reducing property at the CB will be stronger than the undoped $SrTiO_3$. As the codoping of (W, 2N) extends the absorption curve towards visible region in higher extent than that of (Mo, 2N) codoping, (W, 2N)-codoped $SrTiO_3$ should be better choice to achieve improved photocatalytic behavior for solar driven water splitting.

Acknowledgement

We thank the BARC computer centre for providing the high performance parallel computing facility. The authors would like to acknowledge Dr. A. K. Samanta and Dr. M. Kumbhakar for valuable discussions. We also thank Dr. B. N. Jagatap for his encouragement and support. The work of S.K.G. is supported through Sir J.C. Bose Fellowship from the Department of Science and Technology, India.

References:

1 F. E. Osterloh, *Chem. Soc. Rev.,* 2013, **42**, 2294-2320.

2 F. Fresno, R. Portela, S. Su´arezc, and J. M. Coronado, *J. Mater. Chem. A*, 2014, **2**, 2863-2884.

3 T. Hisatomi, J. Kubota, and K. Domen, *Chem. Soc. Rev.* DOI: 10.1039/c3cs60378d (2014).

4 S. Malato, P. Fernández-Ibáñez, M. I. Maldonado, J. Blanco, and W. Gernjak, *Catal. Today,* 2009, **147**, 1-59.

5 A. Di Paola, E. García-López, G. Marcì, and L. Palmisano, *J. Hazard. Mater.*, 2012, **211– 212**, 3-29.

6 A. Kudo, and Y. Miseki, *Chem. Soc. Rev.*, 2009, **38**, 253-278.

7 X. Chen, S. Shen, L. Guo, and S. S. Mao, *Chem. Rev.*, 2010, **110**, 6503-6570.

8 A. Fujishima and K. Honda, *Nature*, 1972, **238**, 37-38.

9 K. Nakata, and A. Fujishima, *J. Photochem. Photobiol. C: Photochem. Rev.*, 2012, **13,** 169-189.

10 J. Shi, and L. Guo, *Prog. Mater. Sci.: Mat. Int*., 2012, **22,** 592- 615.

11 H. Kato, and A. Kudo, *Catal. Lett.*, 1999, **58**, 153-155.

12 B. D. Alexander, P. J. Kulesza, I. Rutkowska, R. Solarska, and J. Augustynski, *J. Mater. Chem*., 2008, **18,** 2298-2303.

13 M. S. Wrighton, A. B. Ellis, P. T. Wolczanski, D. L. Morse, H. B. Abrahamson, and D. S. Ginley, *J. Am. Chem. Soc*., 1976, **98**, 2774- 2779.

14 R. S. Maglizzo, and A. I. Krasna, *Photochem. Photobiol*., 1983, **38**, 15-21.

15 K. Domen, A. Kudo, T. Onishi, N. Kosugi, and K. Kuroda, *J. Phys. Chem*., 1986, **90**, 292- 295.

16 M. S. Wrighton, A. B. Ellis, P. T. Wolczanski, D. L. Morse, H. B. Abrahamson, and D. S. Ginley, *J. Am. Chem. Soc.,* 1976, **98**, 2774- 2779

17 M. Cardona, *Phys. Rev*., 1965, **140**, A 651.

18 Y. Xu, and M. A. A. Schoonen, *Am. Mineral*., 2000, **85**, 543.

189 J. Wang, S. Yin, M. Komatsu, Q. Zhang, F. Saito, and T. Sato, *J. Mater. Chem*., 2003, **13**, 2348-2352.

20 H. W. Kang, and S. B. Park, *Chem. Eng. Sci*., 2013, **100**, 384- 391.

21 N. Li, and K. L. Yao, *AIP. Adv*., 2012, **2**, 032135-10.

22 C. Zhang, Y. Jia, Y. Jing, Y. Yao, J. Ma, and J. Sun, *Comput. Mater. Sci.*, 2013, **79**, 69-74.

23 J. Wang, S. Yin, M. Komatsu, Q. Zhang, F. Saito, and T. Sato, *J. Photochem. Photobiol. A: Chem.*, 2004, **165**, 149-156.

24 Y. Y. Mi, S. J. Wang, J. W. Chai, J. S. Pan, C. H. A. Huan, Y. P. Feng, and C, K. Ong, *Appl. Phys. Lett.*, 2006, **89**, 231922.

25 P. Liu, J. Nisar, B. Pathak, and R. Ahuja, *Int. J. Hydrogen Energy*, 2012, **37**, 11611-11617.

26 Z. Lin, A. Orlov, R. M. Lambert, and M. C. Payne, *J. Phys. Chem. B*, 2005, **109***,* 20948-20952.

27 M. Batzill, E. H. Morales, and U. Diebold, *Phys. Rev. Lett*., 2006, **96**, 026103.

28 Y. Nakano, T. Morikawa, T. Ohwaki, and Y. Taga, *Chem. Phys*., 2007, **339**, 20-26.

29 J. W. Liu, G. Chen, Z. H. Li, and Z. G. Zhang, *J. Solid State Chem*., 2006, **179**, 3704-3708.

30 D. Wang, J. Ye, T. Kako, and T. Kimura, *J. Phys. Chem. B*, 2006, **110**, 15824-15830.

31 W. Wei, Y. Dai, H. Jin, and B. Huang, *J. Phys. D: Appl. Phys*., 2009, **42**, 055401.

32 H. Yu, S. Ouyang, S. Yan, Z. Li, T. Yu, and Z. Zou, *J. Mater. Chem*., 2011, **21**, 11347-11351.

33 P. Reunchan, N. Umezawa, S. Ouyang, and J. Ye, *Phys. Chem. Chem. Phys*., 2012, **14**, 1876-1880.

34 H. Irie, Y. Maruyama, and K. Hashimoto, *J. Phys. Chem. C*, 2007, **111**, 1847-1852.

35 R. Konta, T. Ishii, H. Kato, and A. Kudo, *J. Phys. Chem. B*, 2004, **108**, 8992-8995.

36 H.-C. Chen, C.-W. Huang, J. C. S. Wu, and S.-T. Lin, *J. Phys. Chem. C*, 2012, **116**, 7897-7903.

37 S. W. Bae, P. H. Borse, and J. S. Lee, *Appl. Phys. Lett.*, 2008, **92**, 104107.

38 Y. Gai, J. Li, S.-S. Li, J.-B. Xia, and S.-H. Wei, *Phys. Rev. Lett*., 2009, **102**, 036402.

39 B. Modak, K. Srinivasu, and S. K. Ghosh, *J. Phys. Chem. C*, 2014, **118**, 10711−10719.

40 R. Long, and N. J. English, *Appl. Phys. Lett.* 2009, **94**, 132102.

41 W.-J. Yin, H. Tang, S.-H. Wei, M. M. Al-Jassim, J. Turner, and Y. Yanfa. *Phys. Rev. B*, 2010, **82**, 045106.

42 M. Miyauchi, M. Takashio and H. Tobimatsu, *Langmuir***,** 2004, **20**, 232-236.

43 J. Wang, S. Yin, M. Komatsu, and T. Sato, *J. Eur. Ceram. Soc*., 2005, **25**, 3207-3212.

44 W. Wei, Y. Dai, M. Guo, L. Yu, H. Jin, S. Han, and B. Huang, *Phys. Chem. Chem. Phys.*, 2010, **12**, 7612- 7619.

45 H. Yu, S. Yan, Z. Li, T. Yu, and Z. Zou, *Int. J. Hydrogen Energy*, 2012, **37**, 12120-12127.

46 H. Kato, and A. Kudo, *J. Phys. Chem. B*, 2002, **106**, 5029-5034.

47 T. Ishii, H. Kato, and A. Kudo, *J. Photochem. Photobiol. A: Chem*., 2004, **163**, 181-186.

48 P. Reunchan, S. Ouyang, N. Umezawa, H. Xu, Y. Zhang, and J. Ye, *J. Mater. Chem. A*, 2013, **1**, 4221-4227.

49 Y. F. Shen, T. Y. Xiong, T. F. Li, and K. Yang, *Appl. Catal. B*, 2008, **83**, 177-185.

50 B. F. Gao, Y. Ma, Y. A. Cao, W. S. Yang, and J. N. Yao, *J. Phys. Chem. B*, 2006, **110**, 14391—14397.

51 H. Liu, Z. Lu, L. Yue, J. Liu, Z. Gan, C. Shu, T. Zhang, J. Shi, and R. Xiong, *Appl. Surf. Sci*., 2011, **257**, 9355–9361.

52 M. Li, J. Zhang, and Y. Zhang, *Catal. Commun*., 2012, **29,** 175–179.

53 J. Paier, M. Marsman, K. Hummer, G. Kresse, I. C. Gerber, and J. G. Ángyán, *J. Chem. Phys.*, 2006, **124**, 154709.

54 G. Kresse, and D. Joubert, *Phys. Rev. B*, 1999, **59**, 1758.

55 P. E. Blöchl, *Phys. Rev. B*, 1994, **50**, 17953.

56 J. P. Perdew, J. A. Chevary, S. H. Vosko, K. A. Jackson, M. R. Pederson, D. J. Singh, and C. Fiolhais, *Phys. Rev. B*, 1992, **46**, 6671.

57 H. J. Monkhorst, and J. D. Pack, *Phys. Rev. B*, 1976, **13**, 5188.

58 R. D. Shannon, *Acta Crystallogr.*, 1976, A**32**, 751-767.

59 G. Henkelman, A. Arnaldsson, and H. Jónsson, *Comput. Mater. Sci.*, 2006, **36**, 254– 360.

60 S. Ouyang, H. Tong, N. Umezawa, J. Cao, P. Li, Y. Bi, Y. Zhang, and J. Ye, *J. Am. Chem. Soc.* 2012, **134**, 1974−1977.

61 S. Saha, T. P. Sinha, and A. Mookerjee, *Phys. Rev. B*, 2000, **62**, 8828.

62 R. Long and N. J. English, *Chem. Mater*., 2010, **22**, 1616-1623.

63 W.-J. Shi, and S.-J. Xiong, *Phys. Rev. B*, 2011, **84**, 205210.

Figure Captions

Fig. 1: 2 × 2 × 2 supercell for the cubic $SrTiO_3$ crystal structure. The lattice sites for the dopant elements are indicated by Ti1-Ti3 and O1-O3.

Fig. 2: Density of states of undoped $SrTiO_3$. Vertical dashed line indicates Fermi Level.

Fig. 3: Density of states of N-doped $SrTiO_3$ (a) and (N, N)-doped $SrTiO_3$ (b)

Fig. 4: Density of states of Mo-doped $SrTiO_3$ (a) and W-doped $SrTiO_3$ (b).

Fig. 5: Density of states of (Mo, N)-codoped $SrTiO_3$ (a) and (W, N)-codoped $SrTiO_3$ (b).

Fig. 6: Density of states of (Mo, 2N)-codoped $SrTiO_3$ (a) and (W, 2N)-codoped $SrTiO_3$ (b).

Fig.7: Part of total charge density distribution for (Mo, 2N)-codoped $SrTiO_3$ (a) and (W, 2N)-codoped $SrTiO_3$ (b).

Fig. 8: The calculated VBM and CBM positions of codoped $SrTiO_3$ with reference to that of undoped $SrTiO_3$.

Fig. 9: The calculated absorption curves for the undoped and codoped $SrTiO_3$.

Fig. 10: The variation of defect formation energy with the chemical potential of O (μ_O- $\mu_{O\text{-}gas}$) and Ta (μ_{Ta}- $\mu_{Ta\text{-}bulk}$) for N-doped $SrTiO_3$ (a) Mo-doped $SrTiO_3$ and W-doped $SrTiO_3$ (b) (Mo, 2N)- codoped $SrTiO_3$ (c) (W, 2N)- codoped $SrTiO_3$ (d). The color lines (c) and (d) corresponds to different formation energies for the (Mo, 2N)- codoped $SrTiO_3$ and (W, 2N)- codoped $SrTiO_3$. The codoped system cannot be formed in the lower half of the diagonal axis (large white region) in the case of c and d because the chemical potential of Sr (μ_{Sr}) is exceeded (eq. 7a).

Fig.11: Density of states of (W, 2N)-codoped $SrTiO_3$ using (a) 2 × 1 × 1 supercell, (b) 2 × 2 × 1 supercell, and (c) 2 × 2 × 3 supercell.

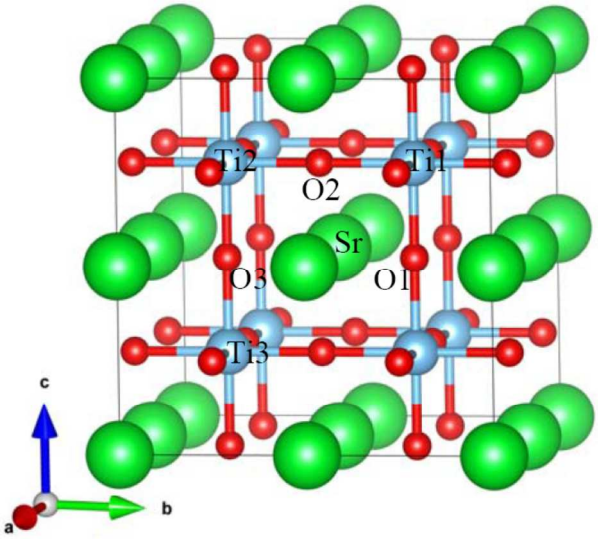

Fig. 1: 2 × 2 × 2 supercell for the cubic $SrTiO_3$ crystal structure. The lattice sites for the dopant elements are indicated by Ti1-Ti3 and O1-O3.

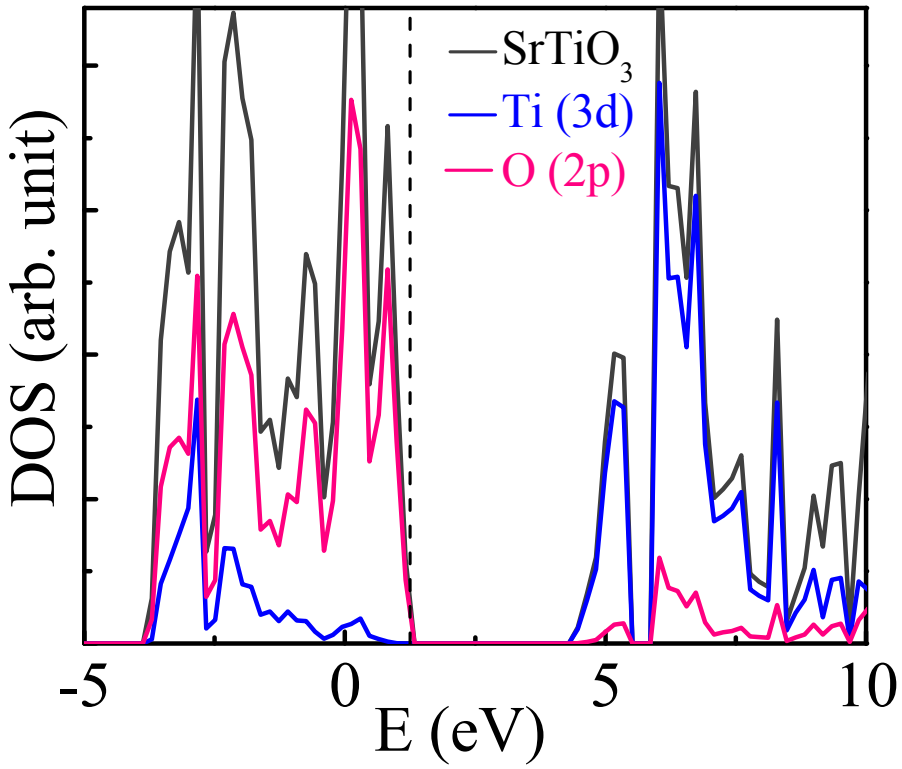

Fig. 2: Density of states of undoped $SrTiO_3$. Vertical dashed line indicates Fermi Level.

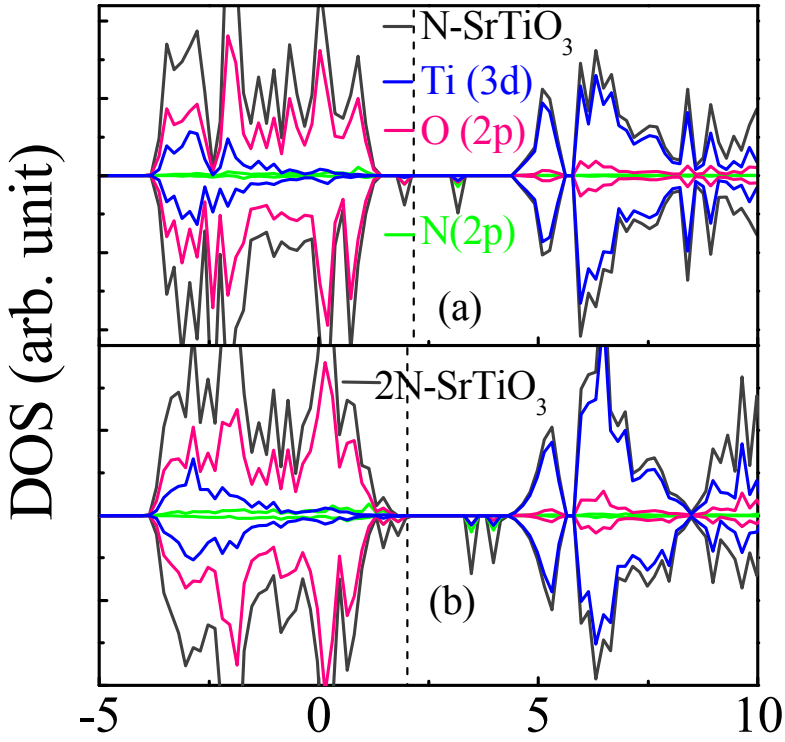

Fig. 3: Density of states of N-doped $SrTiO_3$ (a) and (N, N)-doped $SrTiO_3$ (b)

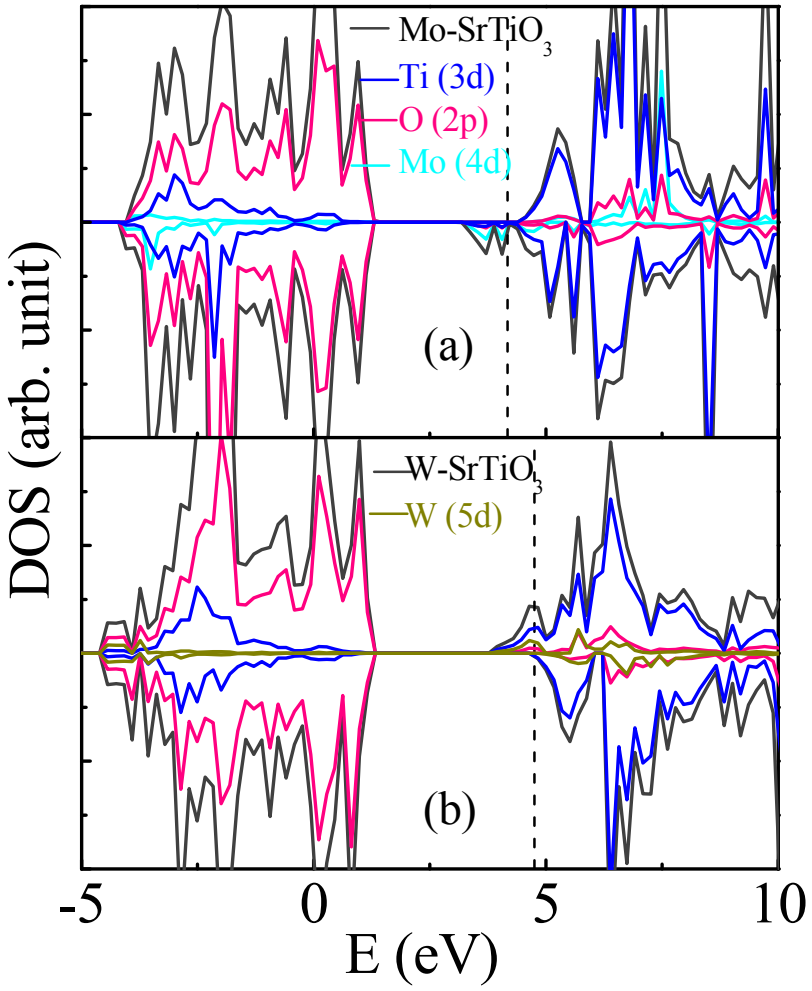

Fig.4: Density of states of Mo-doped $SrTiO_3$ (a) and W-doped $SrTiO_3$ (b).

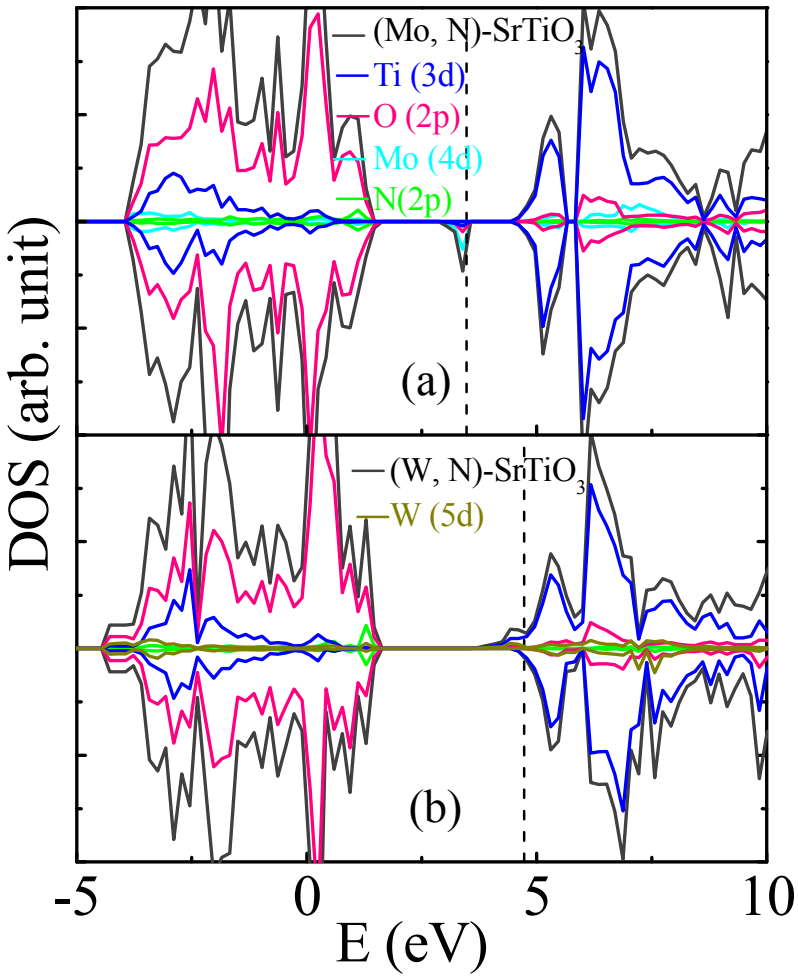

Fig.5: Density of states of (Mo, N)-codoped $SrTiO_3$ (a) and (W, N)-codoped $SrTiO_3$ (b).

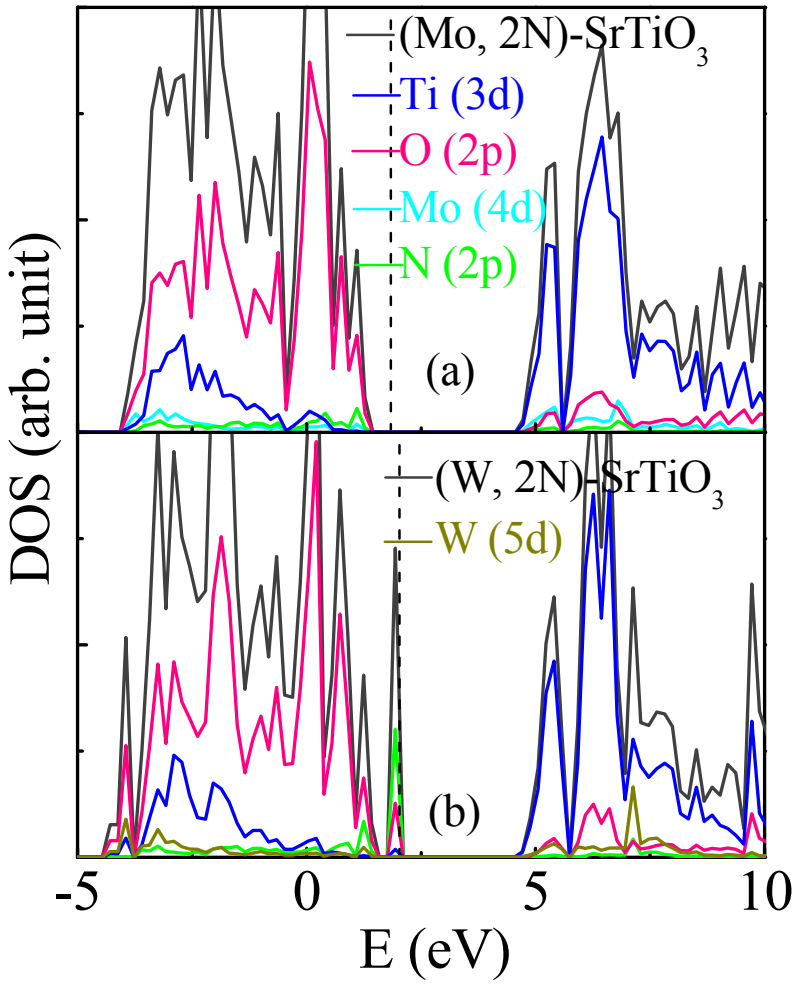

Fig.6: Density of states of (Mo, 2N)-codoped $SrTiO_3$ (a) and (W, 2N)-codoped $SrTiO_3$ (b).

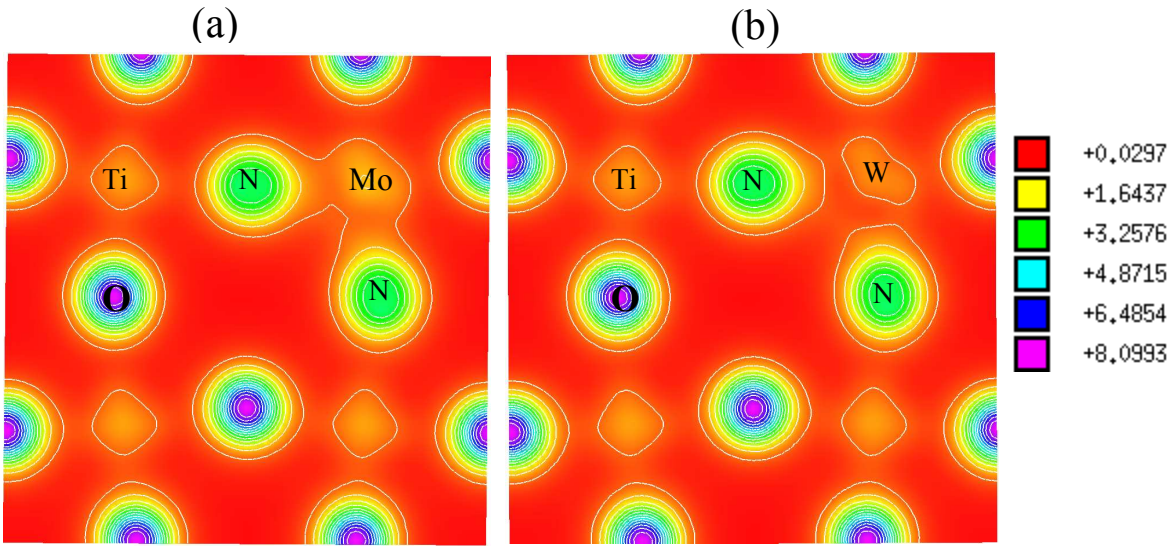

Fig.7: Part of total charge density distribution for (Mo, 2N)-codoped $SrTiO_3$ (a) and (W, 2N)-codoped $SrTiO_3$ (b).

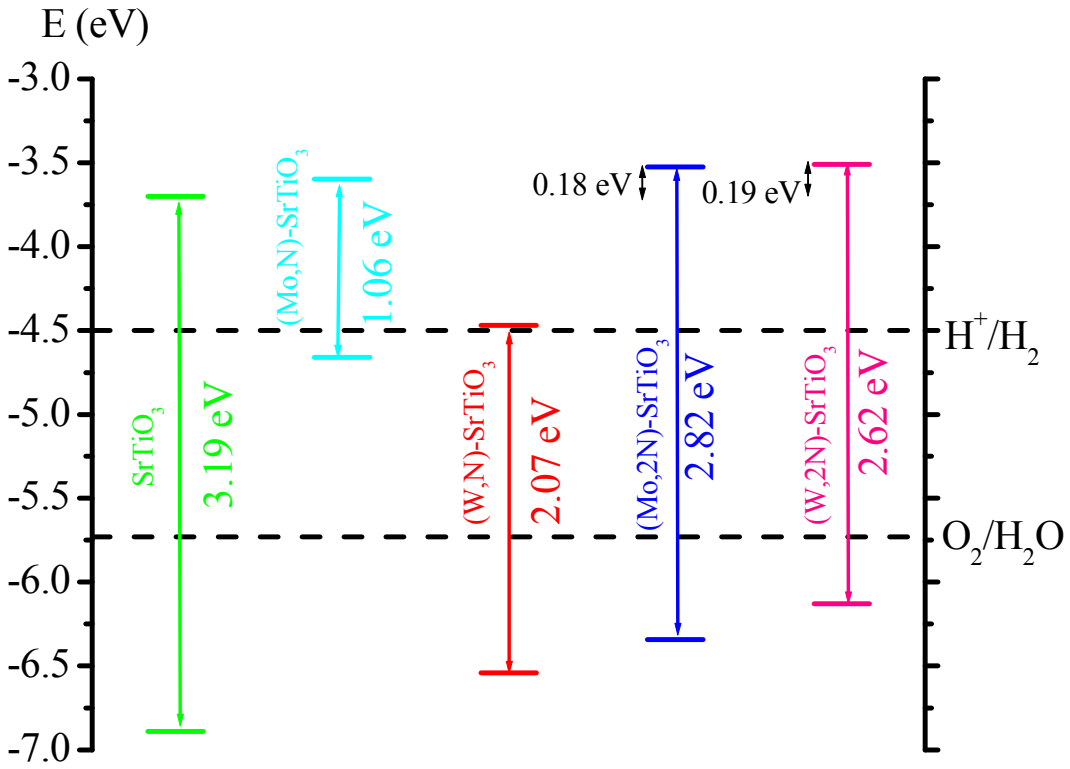

Fig. 8: The calculated VBM and CBM positions of codoped $SrTiO_3$ with reference to that of undoped $SrTiO_3$.

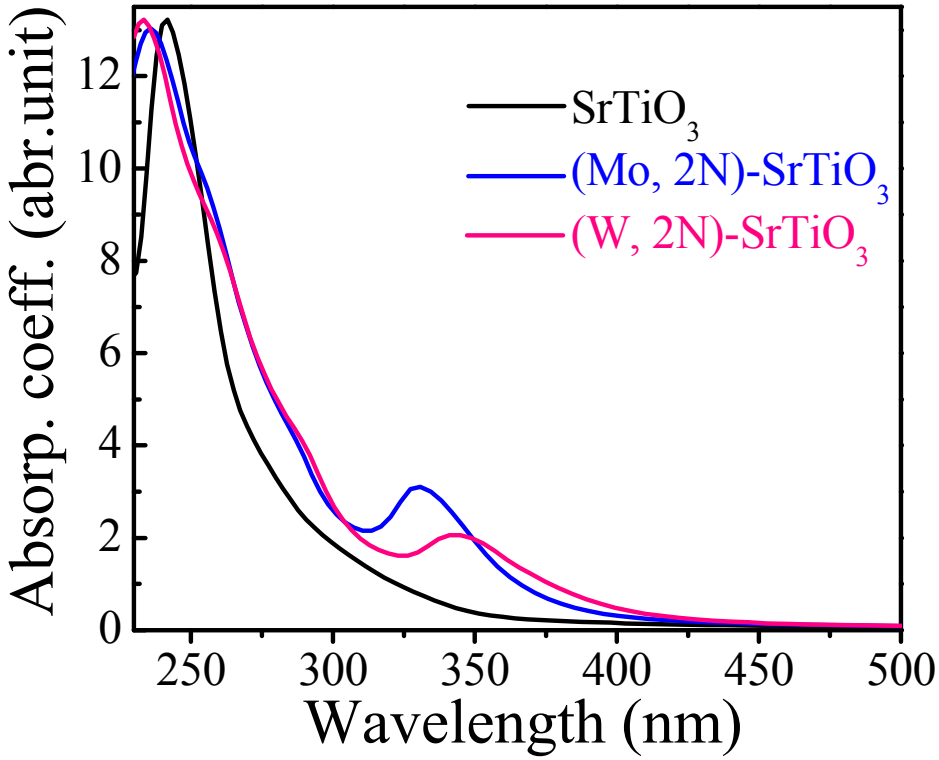

Fig. 9: The calculated absorption curves for the undoped and codoped $SrTiO_3$.

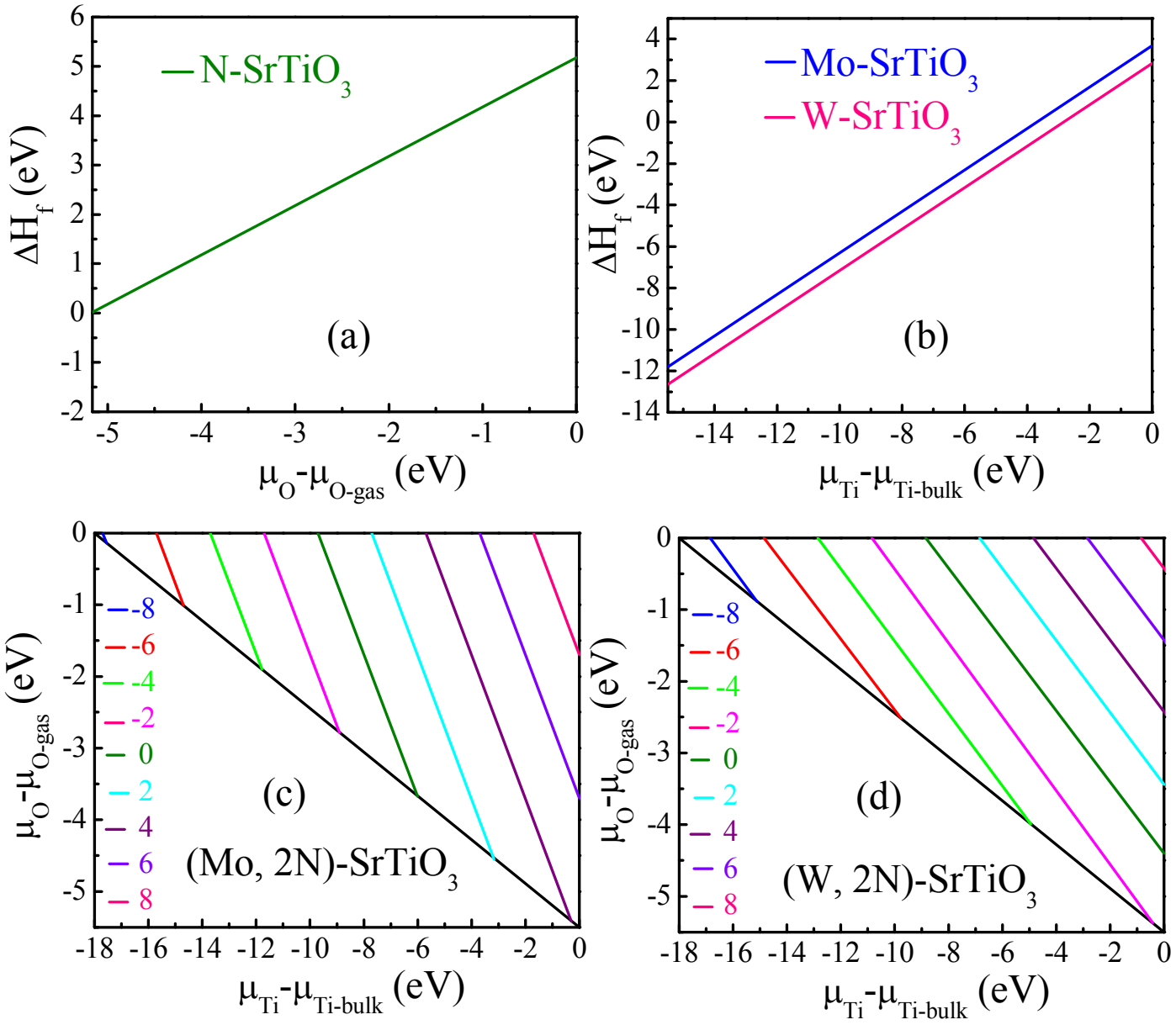

Fig. 10: The variation of defect formation energy with the chemical potential of O (μ_O- $\mu_{O\text{-gas}}$) and Ta (μ_{Ta}- $\mu_{Ta\text{-bulk}}$) for N-doped $SrTiO_3$ (a) Mo-doped $SrTiO_3$ and W-doped $SrTiO_3$ (b) (Mo, 2N)- codoped $SrTiO_3$ (c) (W, 2N)- codoped $SrTiO_3$ (d). The color lines (c) and (d) corresponds to different formation energies for the (Mo, 2N)- codoped $SrTiO_3$ and (W, 2N)- codoped $SrTiO_3$. The codoped system cannot be formed in the lower half of the diagonal axis (large white region) in the case of c and d because the chemical potential of Sr (μ_{Sr}) is exceeded (eq. 7a).

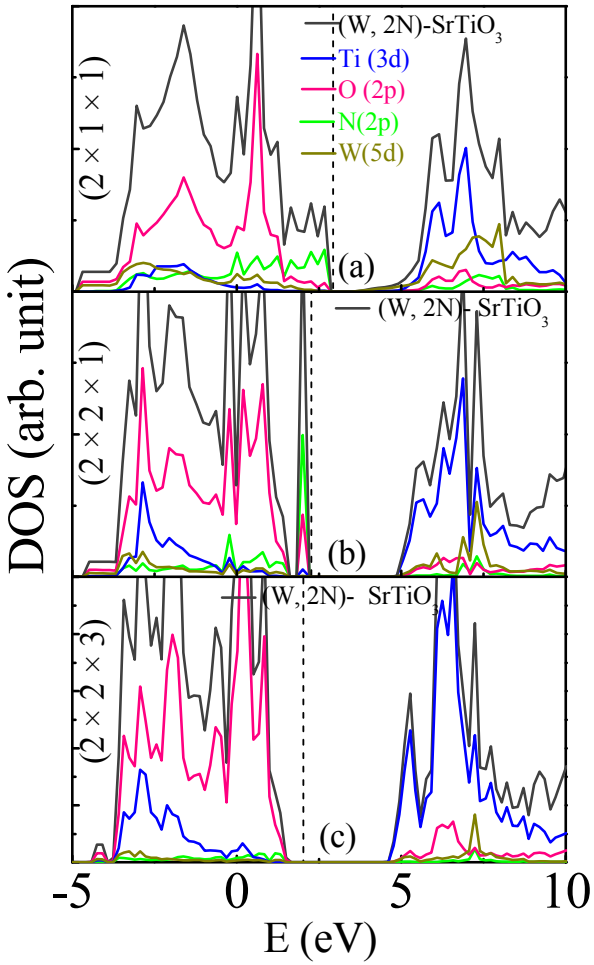

Fig.11: Density of states of (W, 2N)-codoped $SrTiO_3$ for (a) 2 × 1 × 1 supercell, (b) 2 × 2 × 1 supercell, and (c) 2 × 2 × 3 supercell.